

**Thermoelectric Properties of the Heterostructural
Alloy $Sn_{1-x}Ca_xSe$**

Michael Forkner

Advisor: Dr. Janet Tate



A thesis presented for the degree of
Bachelor's of Science

Department of Physics
Oregon State University
May 12th, 2017

Acknowledgments

I would like to thank my PI, Dr. Janet Tate for allowing me to conduct my research in her laboratory. I would also like to thank graduate student Bethany Matthews for teaching me how to use the equipment, creating the samples, help with data analysis, and general help at all stages of this process. James Haggerty taught me how to use the Raman spectroscopy system and analyze the data. Dr. Aaron Holder and Dr. Stephan Lany at NREL created the theoretical material. Thank you to the OSU Physics Department for providing my physics education. This work was supported as part of the Center for the Next Generation of Materials by Design, an Energy Frontier Research Center funded by the U.S. Department of Energy, Office of Science.

Contents

1	Introduction	1
1.1	Background	1
1.2	Motivation	1
1.3	SnSe and CaSe	1
2	Theory	2
2.1	Metastability and Alloying	2
2.2	Hall Effect	3
2.3	Thermoelectric Effect	4
2.4	Power Factor	6
2.5	Raman Spectroscopy	6
3	Methods	7
3.1	Thin Film Deposition	7
3.2	Electrical Film Characterization	7
3.2.1	Thermoelectric Effect	7
3.2.2	Hall Effect	8
3.3	Raman Characterization	9
4	Results and Discussion	9
4.1	Seebeck Coefficient	9
4.2	Carrier Density	10
4.3	Resistivity	12
4.4	Power Factor	13
4.5	Comparison to Theoretical Band Gap Analysis	14
4.6	Alloyed Films	14
4.7	Phase Separated Films	15
4.8	Raman Spectroscopy	16
5	Conclusion	16

List of Figures

1.1	Structures of SnSe and CaSe	2
2.1	Energy States in a Metastable Material	2
2.2	Theoretical Stability Curves and Phase Transition Line	3
2.3	Electron Transport and the Hall Voltage	4
2.4	Carrier Travel in N-type and P-type Semiconductors	5
2.5	Simplistic Thermocouple	5
2.6	Raman Scattering from an Incident Light Ray	6
3.1	PLD and Layer growth of $Sn_{1-x}Ca_xSe$ Films	7
3.2	Schematic Diagram of the Room Temperature Seebeck System	8
3.3	Experimentally Preferred Hall Geometries	8
4.1	Seebeck Coefficient of the Alloyed Films as a Function of Calcium Doping Concentration	9
4.2	Seebeck Coefficient of the Phase Separated Films as a Function of Calcium Doping Concentration	10
4.3	Carrier Density of the Alloyed Films as a Function of Calcium Doping Concentration	11
4.4	Carrier Density of the Phase Separated Films as a Function of Calcium Doping Concentration	11
4.5	Resistivity of the Alloyed Films as a Function of Calcium Doping Concentration	12
4.6	Resistivity of the Phase Separated Films as a Function of Calcium Doping Concentration	12
4.7	Power Factor of the Alloyed Films as a Function of Calcium Doping Concentration	13
4.8	Power Factor of the Phase Separated Films as a Function of Calcium Doping Concentration	13
4.9	Band Gap of the Alloyed Films as a Function of Calcium Doping Concentration	14
4.10	Raman Spectra of the CaSnSe Target Pre- and Post-Anneal	16

Abstract

By alloying face centered cubic *CaSe* with orthorhombic *SnSe*, we created the heterostructural alloy $Sn_{1-x}Ca_xSe$. The phase separated films created with a high deposition temperature acted as highly crystalline *SnSe* while the low deposition temperature films acted as a mix of *SnSe* and *CaSe*. For the alloyed films we observed a change in the Seebeck coefficient, carrier density, and resistivity across the theoretically predicted phase transition between the orthorhombic and cubic structures of the alloy. Across the phase transition line, there is a decrease in resistivity from 10^1 to $10^{-2} \Omega cm$, a significant increase in the carrier density from 10^{17} to $10^{21} cm^{-3}$, and a decrease in the Seebeck coefficient from 400 to $40 \mu V/K$. At the phase transition composition, there is the maximum in the carrier density and the minimum in the resistivity and Seebeck coefficient due the non-linear change in the properties as a function of the calcium concentration. This non-linear scaling of the properties suggests a new avenue for manipulating semiconductor properties using heterostructural alloying.

1 Introduction

1.1 Background

The focus of this work is to characterize the properties of the semiconductor alloy calcium tin selenide ($Sn_{1-x}Ca_xSe$). This alloy, made from tin selenide (SnSe) and calcium selenide (CaSe), is a thin film semiconductor. Semiconductors are essential to modern day electronics. The challenge in today's world is making these electronics more efficient, powerful, and cheaper. By using heterostructural alloying, it is possible to design and create new semiconductors with properties that were out of reach by the conventional means of isostructural alloying.

1.2 Motivation

This work is directed by the Center for Next Generation Materials by Design (CNGMD). The overarching goal of this project is to study metastability in alloys. Metastability is a tool which can control the structure and properties of materials. Metastability, in the form of alloying, can provide fine tuning of the band gap and thermoelectric properties. Another goal for the project is to change from an experimentally driven model to a computationally driven model. Most experimentalists pick materials they think might produce desirable properties based on their previous knowledge or research. This method, which often yields new and interesting materials, sometimes fails to create anything useful. This leads to waste of precious time and resources. Instead, the goal is to get experimentalists to work closer with theoreticians. With computing power becoming cheaper, the theoreticians can efficiently identify what materials will produce the desired properties, with less waste of resources. Then an experimentalist will test these materials and determine if they are in fact what the theoreticians calculated. The final goal being that one can choose certain properties and have the computationalists calculate what materials will provide those properties, and give insight in the necessary growth conditions.

On this project we are looking at the electrical properties of a metastable heterostructural alloy. Two different semiconductors, each with different crystalline lattices, are alloyed together to form one homogeneous heterostructural alloy. Since we are creating a single stabilized phase of the crystal, there will be a concentration of the alloy where the structure will change from that of its first end member (orthorhombic) to that of its second (cubic). We are looking to study this change in phase and how it affects the properties of the alloy. To determine the properties of the sample, we will measure the thermoelectric effect, the resistivity, and the carrier concentration at different concentrations of calcium. Heterostructural alloying could be an extremely important tool in manipulation of a material's properties to allow for maximized efficiency.

1.3 SnSe and CaSe

The two semiconductors used to create this heterostructural alloy are tin selenide (SnSe) and calcium selenide (CaSe). SnSe is a well known semiconductor with a orthorhombic structure. An orthorhombic structure is one in which each lattice constant in the unit cell has a different value ($a \neq b \neq c$), yet all the angles between the atoms are 90 degrees relative to one another. This is shown on the left in Figure 1.1. CaSe is also a well known insulator and has a rock salt structure. A rock salt, or face-centered cubic structure, has all crystalline lattice constants the same ($a = b = c$) with atoms on the 8 corners of a cube and one on each face. Each atom is connected to the six atoms around it with atoms alternating between calcium and selenium. CaSe has a much larger band gap, around 4.5 eV, than SnSe which has a band gap of 1 eV. SnSe is a widely studied semiconductor because of its merit (zT) and power factor (PF). SnSe has a zT of 2.6 at high temperatures [9]. Previously *PbTe* had the highest known zT for any semiconductor, around 1 [6]. Crystalline SnSe has a power factor of order $10^4 \mu V^2 / \Omega K^2$ at room temperature, a relatively large value. For thermoelectric applications, a large power factor is highly desirable.

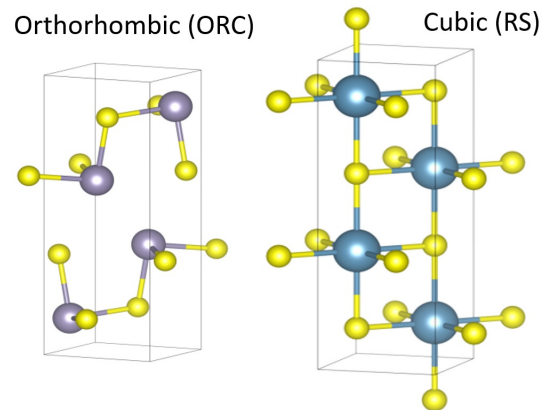


Figure 1.1: Structures of SnSe (left) and CaSe (right) [7]

2 Theory

2.1 Metastability and Alloying

A metastable state is a state that is a local minimum in energy landscape, but not in its most energetically favorable configuration. This means that small perturbations will not upset the state, but large ones will cause it to go to its lowest energy state. Figure 2.1 is the simplest view of metastability. A particle in state E_1 is metastable and will not immediately relax to state E_0 , even though state E_0 is the ground state of the system. The particle in state E_1 has to have an added energy or perturbation equal to E_{01} to allow it the energy to then ‘relax’ to state E_2 . Metastable materials are very common in certain types of crystals. Diamond, for example, is a metastable form of carbon. The crystalline carbon lattice that is diamond has a high energy associated with it, and carbon's preferred form is the lower energy graphite phase. Although, once in the diamond phase, the carbon will not relax to graphite without a large energy input to the system. Not only are the structures of carbon different between diamond and graphite, but the thermoelectric and optical properties are different. For example, diamond is an insulator while graphite is an excellent conductor [8]. Metastable materials are also present in other forms, including polymers and isomers.

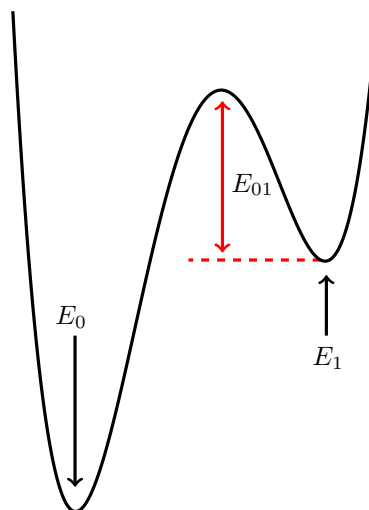


Figure 2.1: Energy States in a Metastable Material

The heterostructural alloys that are studied in this thesis are examples of metastable structures. Unlike isostructural alloying, heterostructural alloying has end members with different phases (crystalline lattice structures). Since we are trying to form one homogeneous alloy, we must force the combination of the two end members into one phase. This requires added energy to stabilize the crystalline structure in the metastable state. For anything but a pure concentration of one of the end members, the material will be in a non-relaxed energy state.

Figure 2.2 shows the enthalpy of mixing, calculated by Lany and Holder, of both the cubic (blue line) and orthorhombic (red line) phases as a function of calcium concentration. The enthalpy of mixing is the theoretically calculated energy that is required above the ground state to form the homogeneous heterostructure, either cubic or orthorhombic, at the desired calcium concentration. This plot shows the phase transition from the homogeneous cubic phase to the homogeneous orthorhombic phase. Where the orthorhombic enthalpy of mixing is lower than the cubic enthalpy of mixing, the structure will more likely crystallize into the metastable orthorhombic phase. When the enthalpy of mixing is lower in the cubic phase than the orthorhombic phase, the structure will crystallize into the metastable cubic phase. The theoretical phase transition is where the two enthalpies are equivalent. Any small deviation in the calcium concentration at the phase transition (theory: $x = 0.125$), will lead to either the cubic or the orthorhombic phase being formed.

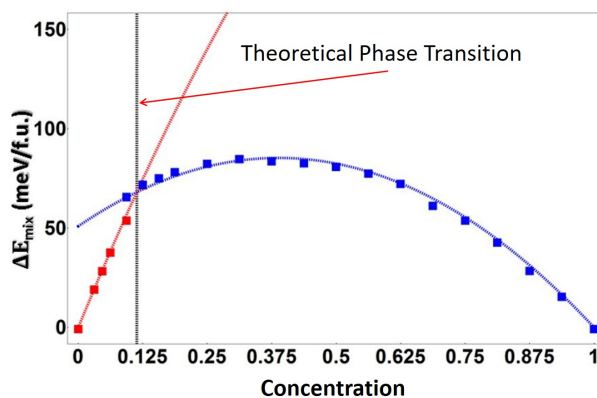


Figure 2.2: Theoretical Stability Curves and Phase Transition Line. Blue/Red lines: The Energy to Stabilize in Orthorhombic/Cubic Configuration Respectively [7]

2.2 Hall Effect

The Hall effect, discovered by Edwin Hall, is the generation of a voltage when you apply mutually perpendicular current and magnetic fields. This voltage, called the transverse voltage, is created in the 3rd mutually perpendicular direction from both the current and the magnetic field, as seen in Figure 2.3.

A current is induced through the sample, electrons will then flow in the opposite direction of that induced current, while holes will flow in the direction of the current. Next, an external magnetic field is applied. The Lorentz force then causes the carriers to travel to one side. This movement of the carriers creates an electric potential. This generated potential is the transverse hall potential. By determining the sign of the transverse potential, the type of carriers in the sample is determined.

It is also possible to use measurements from multiple different sample connections at multiple different magnetic field strengths to determine the resistivity, mobility, carrier concentration, and the hall coefficient R_H through these relations:

$$V_H = \frac{IB}{qnd} \quad (2.1)$$

$$R_H = \frac{1}{nq} \quad (2.2)$$

Where V_H is the transverse hall voltage, I is the current, B is the strength of the magnetic field, q is the charge of the carrier (either a hole or an electron), n is the carrier density, and d is the thickness of the sample, typically found using optical techniques.

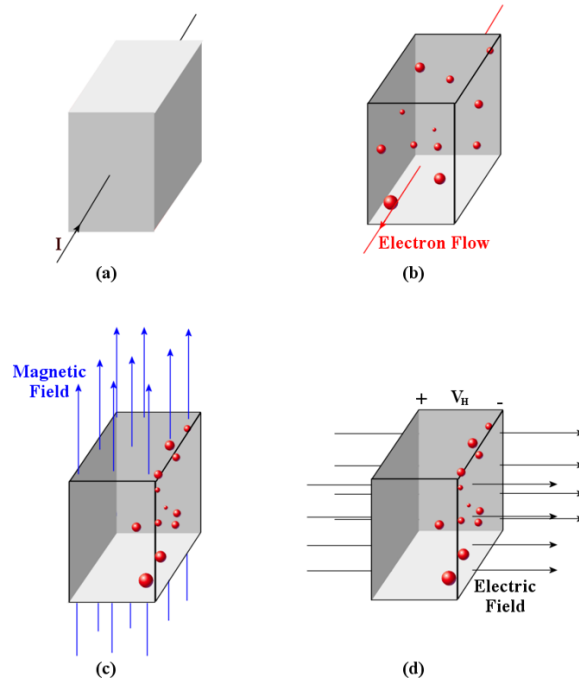


Figure 2.3: Electron Transport and the Hall Voltage [2]

2.3 Thermoelectric Effect

The thermoelectric effect, also known as the Seebeck effect, is the voltage generated between two dissimilar metals (or semiconductors) when a temperature gradient is applied. When a temperature gradient is applied across the sample, energy is added to one side. This added energy excites the carriers and they diffuse to the energy states that minimize the electric potential energy. This in turn creates an electric field which produces a voltage across the sample. This process is shown below in Figure 2.4.

The Seebeck coefficient is the quantitative measurement of the thermoelectric effect. It is the ratio of the voltage difference to the temperature difference.

$$S = -\frac{\Delta V}{\Delta T} \quad (2.3)$$

The negative sign in Eq. 2.1 comes from a convention about the differences:

$$S = \frac{-(V_{hot} - V_{cold})}{T_{hot} - T_{cold}} = \frac{V_{cold} - V_{hot}}{T_{hot} - T_{cold}} \quad (2.4)$$

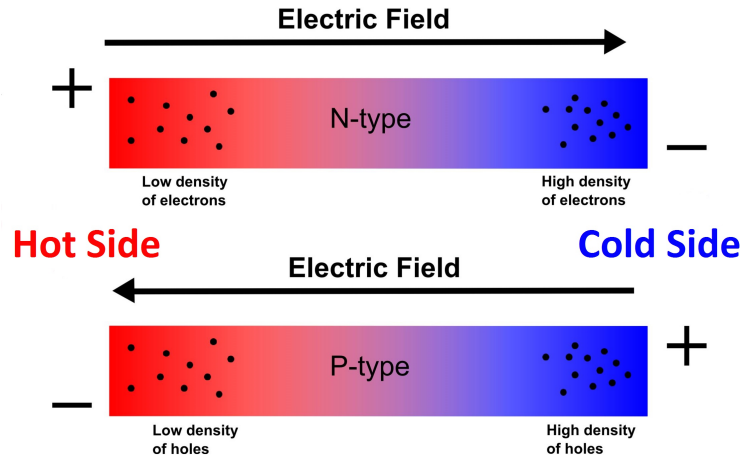


Figure 2.4: Carrier Travel in N-type and P-type Semiconductors [1]

Convention defines a positive Seebeck coefficient to have the positive carriers (holes) moving through the sample. So, if holes are moving through the sample, then $T_{hot} - T_{cold} > 0$ and $V_{hot} - V_{cold} < 0$, therefore an additional negative sign is needed to define the Seebeck coefficient. Thus the voltage in the sample is always opposite to the direction of thermal gradient for positive Seebeck values (p-type carriers), and is in the same direction for negative Seebeck values (n-type carriers).

The thermoelectric effect relates heat and electricity allowing for applications include thermoelectric generators and temperature measurement.

Thermoelectric generators take advantage of temperature gradients that occur naturally or are part of an existing process. There are thermoelectric generators inside the earth's core, in power plants to convert waste heat to more power, and even in cars to increase their efficiency. Thermoelectric generators are not widely used because they are inefficient a maximum of efficiency of 44.5%, but if there is a large temperature gradient present it is easier to convert it to electricity [5].

The thermoelectric effect is also an effective and accurate way of measuring temperature difference. Figure 2.5 shows a thermocouple, a device with junctions between two metals with different Seebeck coefficients. A current flows in the loop if the junctions are at different temperatures. Alternatively, the circuit can be broken and the voltage measured. If the temperature of one junction is known, the temperature of the second can be determined (an absolute thermocouple). If neither temperature is known, only the temperature difference between the two points is known (a differential thermocouple).

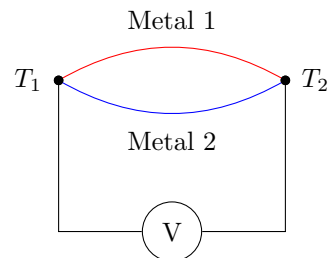


Figure 2.5: A Thermocouple is any Two Metals Connected at Their End Points

2.4 Power Factor

The power factor is a number that describes the overall relationship of the thermoelectric properties and the conductivity. It is defined as:

$$PF = \frac{S^2}{\rho} \quad (2.5)$$

Where S is Seebeck coefficient and ρ is the resistivity. The power factor is useful as a quick tool to determine the potential thermoelectric uses of the semiconductor. A high power factor is desirable because it means that the semiconductor has a large Seebeck coefficient while retaining a large conductivity, two properties that normally are inversely related. Metals have high conductivity but low Seebeck coefficients; semiconductors and insulators have medium to small conductivities but large Seebeck coefficients. Since the power factor is proportional to the square of the Seebeck coefficient, but only the first power of the conductivity, the goal is to try to maximize the Seebeck coefficient while minimizing the loss in conductivity. This will result in a sample with desirable thermoelectric properties that has potential in industrial applications.

2.5 Raman Spectroscopy

Raman spectroscopy uses the inelastic scattering of light to determine crystalline structure. As the incident photons pass through the sample, they interact with the quantum vibrational modes of the lattice. This results in inelastic scattering of the photon, changing its energy. The intensity of the scattered light is graphed as a function of the shift in wavenumber [cm^{-1}], producing a unique spectrum which is characteristic of each crystal structure.

Figure 2.6 shows incident light (green) and three reflected beams (green, blue, and red). The blue beam represents light that gains energy from the lattice vibrations and the wavelength shortens (anti-Stokes scattering). The red beam represents light that lost energy to the lattice vibrations and the wavelength lengthens (Stokes scattering). The green beam is elastically scattered (Rayleigh scattering) and does not lose energy to the lattice, it simply changes direction. Rayleigh scattering is what is generally observed in everyday life.

Raman spectroscopy is similar in some respects to the more familiar x-ray diffraction, which also produces a unique signature of a crystal structure. X-ray diffraction is an elastic scattering process, and because the x-ray wavelength is similar to the atom spacing (a few Angstrom), the interference effects produce sharp spots at specific angles that are characteristic of the crystal structure. Unlike X-Ray spectroscopy, Raman spectroscopy resolves images on the micron scale. This allows determination of the crystalline structure at specific points across the sample. One of the downsides of Raman spectroscopy is that, due to destructive interference in the lattice, cubic structures have very weak to non-existent Raman spectra.

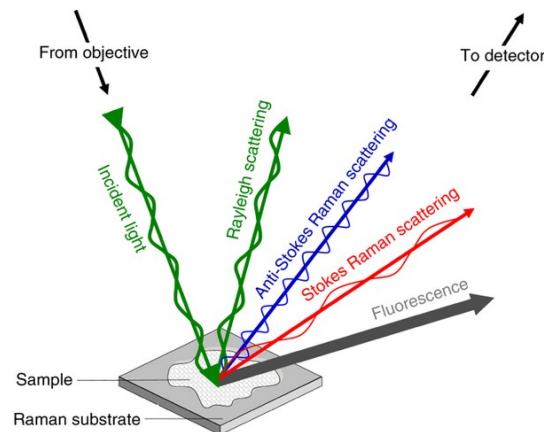


Figure 2.6: Raman Scattering from an Incident Light Ray [4]

3 Methods

3.1 Thin Film Deposition

The films are grown using Pulsed Laser Deposition (PLD) in ultra-high vacuum. Samples are prepared on a fused silica (SiO_2) substrate by growing small layers of SnSe and CaSe on the substrate as shown in Figure 3.1b. Each layer is 50 laser pulses at the selected laser fluence (energy), $1 J/cm^2$. The laser is a 248 nm Lambda Physik with a repetition rate of 10 Hz. Figure 3.1a shows the inside of the vacuum chamber where the films are grown. Referring to Figure 3.1a the laser comes in (1) and strikes the target (2), either pure SnSe or CaSe, and ablates some of the material. This ablated material creates a plume (3) which lands on the fused silica substrate (4). The target is set on a rotating stand as to prevent boring a hole in one place. To achieve homogeneous mixing and to stabilize the crystalline phase in a metastable state, the substrate is kept between 220 and 515 degrees Celsius. Varying the deposition parameters, laser fluence, substrate temperature, number of pulses, and calcium concentration allowed fine tuning to produce heterostructural alloys more reliably. Deposition of the samples was preformed by graduate student Bethany Matthews.

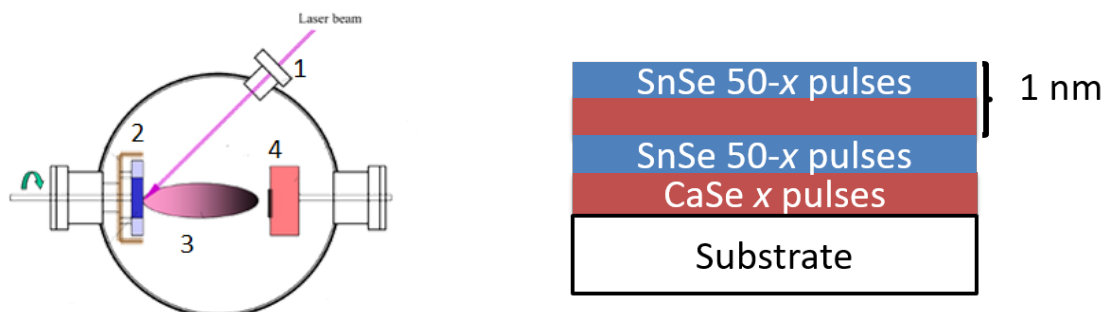


Figure 3.1: (a): Schematic of the PLD Chamber (b): Layer Growth of $Sn_{1-x}Ca_xSe$ Films

3.2 Electrical Film Characterization

3.2.1 Thermoelectric Effect

Figure 3.2 is a schematic diagram of the Seebeck setup used. Two copper blocks serve as the base and are electrically isolated from outside systems. The voltage difference between the two copper blocks is measured by a Tektronix DM 5120. This voltage difference is generated by the temperature gradient across the sample. Also attached to the two copper blocks is a type K thermocouple. Type K thermocouples are made from chromel (90/10 Nickel-Chromium) and alumel (95/2/2/1 Nickel-Manganese-Aluminum-Silicon), and have a Seebeck coefficient of approximately $40 \mu V/K$ at room temperature. The thermocouple must be placed into thermal, but not electrical, contact with the blocks. This is done by drilling holes into the block, and using a thermally conducting plastic to cover the wires. The type K thermocouple alumel leads are then connected to copper leads and fed into a Keithley 195A digital multimeter (DMM) to measure the voltage produced. The $40 \mu V/K$ is then used as a conversion from voltage to temperature difference. To heat the blocks and create the temperature difference across the sample, a 20Ω resistor is placed in thermal contact with the 'hot' block. The current to heat the resistor is supplied by a Keithley 2400 source meter. Indium leaflets are placed onto the copper blocks to aid in electrical contact with the sample. The sample is then placed over the indium leaflets and an electrically insulated plate is screwed down over the sample press the sample into the indium leaflets and improve contact. A hand held DMM is used to measure the resistance of the system to ensure proper contact is made. A LabVIEW program remotely sets the current through the resistor and creates a temperature difference of five Kelvin. As the temperature difference returns to equilibrium, it records the thermocouple voltage μV and voltage generated across the sample. It then converts the thermocouple voltage to a temperature difference, and plots the temperature difference against

the voltage generated. The slope of this linear plot is the Seebeck coefficient in $\mu V/K$. Chromel and alumel wires, whose Seebeck coefficients are 18 and $-22 \mu V/K$ respectively, are used to check that the setup is calibrated properly.

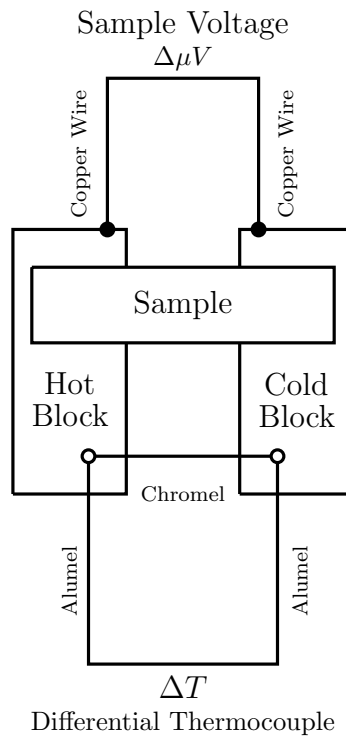


Figure 3.2: Schematic Diagram of the Room Temperature Seebeck System. Solid circles represent electrically conductive connections, open circles represent electrically isolated, thermally conductive connections

3.2.2 Hall Effect

Theoretically, any Hall geometry will work to measure the Hall effect. All that is necessary is the sample be a closed solid surface with four connections on the outside. Experimentally, making any contact adds in resistance and uncertainty to the measurement. To minimize the added uncertainty, one can use specific geometries. Figure 3.3 shows some of the common Hall geometries. The measurement geometry used for the results of this project was a slightly modified cloverleaf in the Van Der Paw configuration, Figure 3.3a.

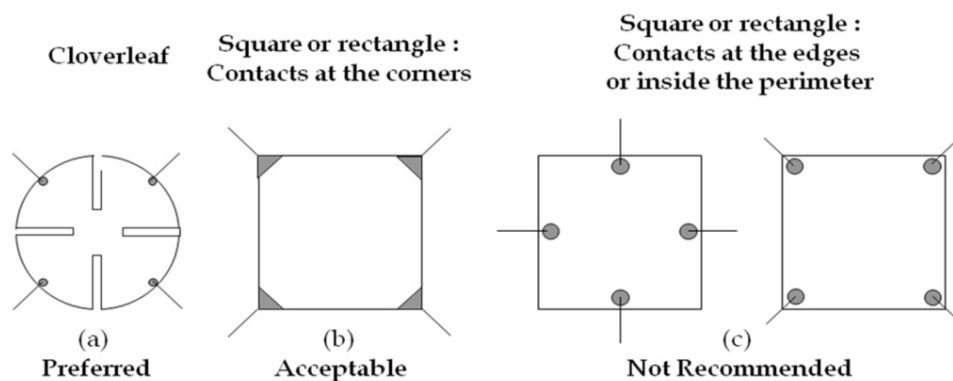


Figure 3.3: Experimentally Preferred Hall Geometries [3]

Contacts are made with indium leaf using a soldering iron. Indium, preferred over tin-lead solder, provides the best ratio of electrical conductivity to added sample resistance. The contacts are made on the four points equidistant from each other on the edge of the sample and connect to a board that then is plugged into the LakeShore Hall Measurement system. The sample and board are then encased in a metal sheath that minimizes any stray electromagnetic fields, and lowered between two electromagnets. A magnetic field probe is placed between the electromagnet to obtain a precise measurement of the field applied to the sample. The program is then run to collect voltage data from a current induced across all linear combinations of the sample connections. This is repeated for each value of the magnetic field from -10 to 10 *kG* in steps of 1 *kG*.

3.3 Raman Characterization

Raman characterization uses a 532 nm laser to measure the shift in the energy of reflected light. First, a pure silicon sample on an amorphous substrate is used to ensure the wavelength of the laser. The measured spectrum of the silicon is then matched against the known spectrum. Next, the substrate of the sample is measured to obtain a background spectrum to later subtract from the spectrum of the sample. The background spectrum is normalized and saved into the program. The sample is then loaded into the system and a spectrum is taken. The laser takes three measurements, each one 10 seconds long. The spectrum is then averaged and normalized. The background is subtracted, and a polynomial peak fit is applied. This spectrum is then compared to known spectra of different materials to determine what structure and composition the sample is.

For the $Sn_{1-x}Ca_xSe$ films, the 532 nm laser was too intense initially. This resulted in degradation of the sample in the form of burn marks and structural deformation. To lower the energy, a smaller iris and a larger filter were used to lower the intensity.

4 Results and Discussion

4.1 Seebeck Coefficient

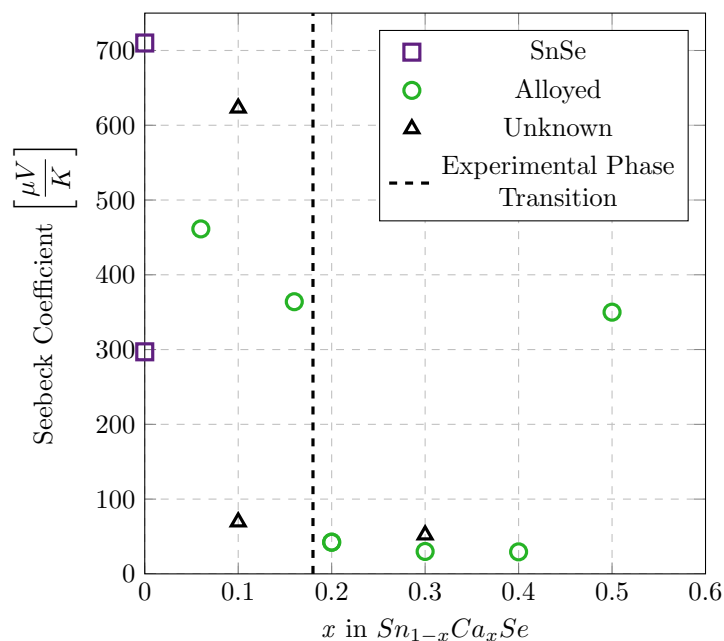


Figure 4.1: Seebeck Coefficient of the Alloyed Films as a Function of Calcium Doping Concentration

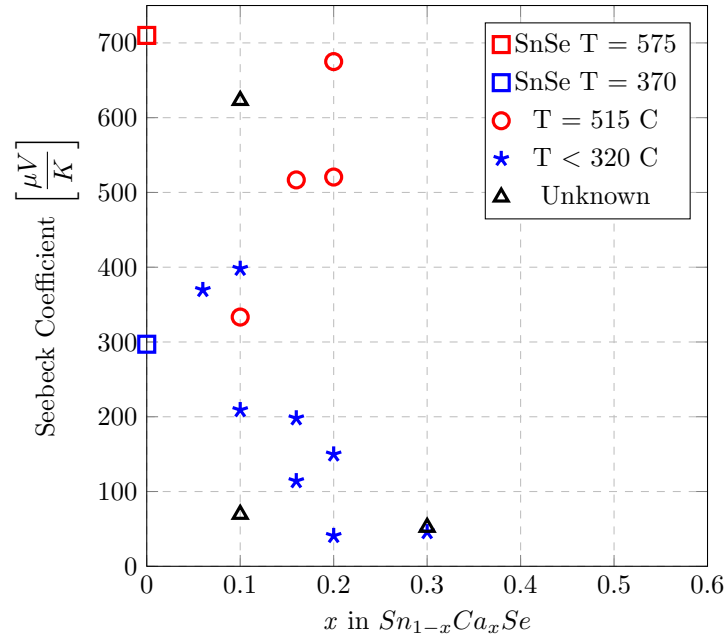


Figure 4.2: Seebeck Coefficient of the Phase Separated Films as a Function of Calcium Doping Concentration

Figure 4.1 is the thermoelectric response for the alloyed films as a function of calcium concentration x . The Seebeck coefficient is originally a downward slope, and then as it crosses the phase transition line, it decreases discontinuously, and then increases with calcium concentration. Measuring samples over 50% calcium concentration was impossible due to high resistivity and faster sample degradation.

Figure 4.2 is the thermoelectric response for the phase separated films as a function of calcium concentration x . There are two distinct trends for the phase separated films, dependent on the deposition temperature. The high deposition temperature films increase as a function of calcium concentration, and the low temperature decrease as a function of the calcium concentration.

4.2 Carrier Density

Figure 4.3 is the carrier density of the alloyed films as a function of calcium concentration x . Pure $SnSe$ has a relatively high carrier density at around $10^{17}cm^{-3}$. The carrier density initially decreased with calcium concentration, only to increase drastically around the phase transition line. Carrier concentrations above $10^{20}cm^{-3}$ are rare in semiconductors and are more indicative of metals.

Figure 4.4 is the carrier density of the phase separated films as a function of calcium concentration x . The high temperature films are around the same carrier density as the pure $SnSe$ film, while the low temperature films have many more free carriers.

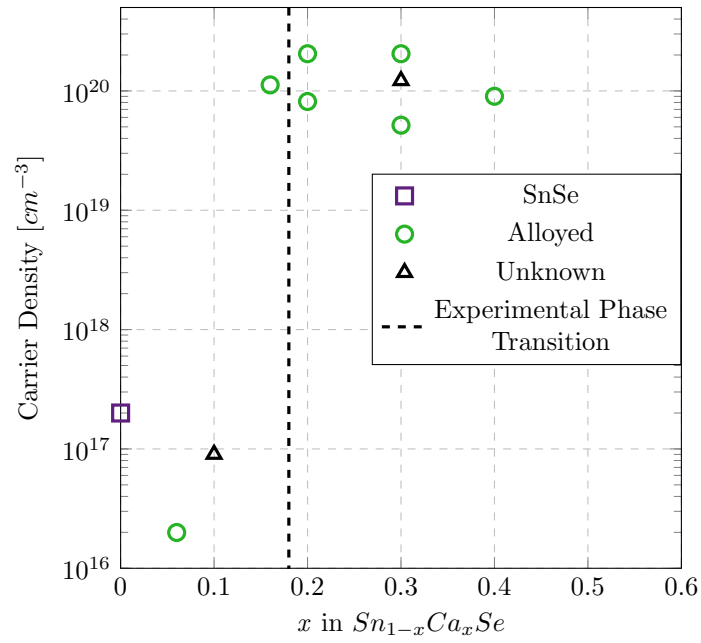


Figure 4.3: Carrier Density of the Alloyed Films as a Function of Calcium Doping Concentration

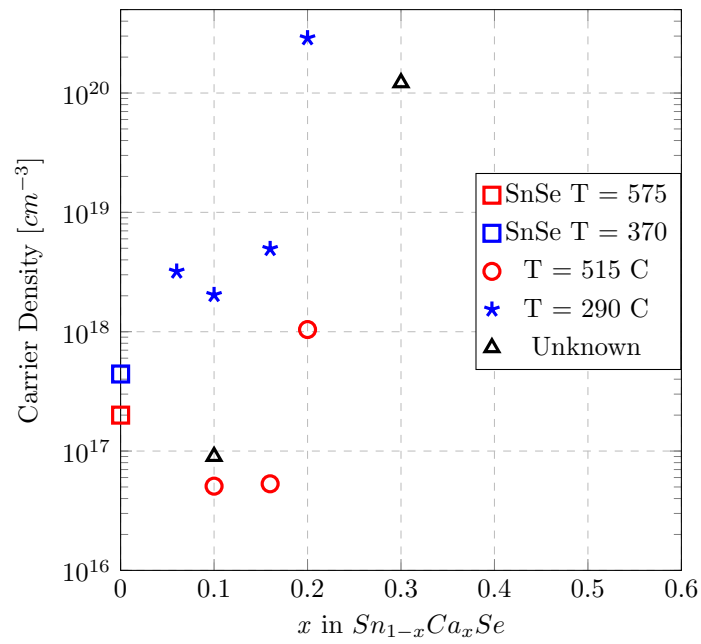


Figure 4.4: Carrier Density of the Phase Separated Films as a Function of Calcium Doping Concentration

4.3 Resistivity

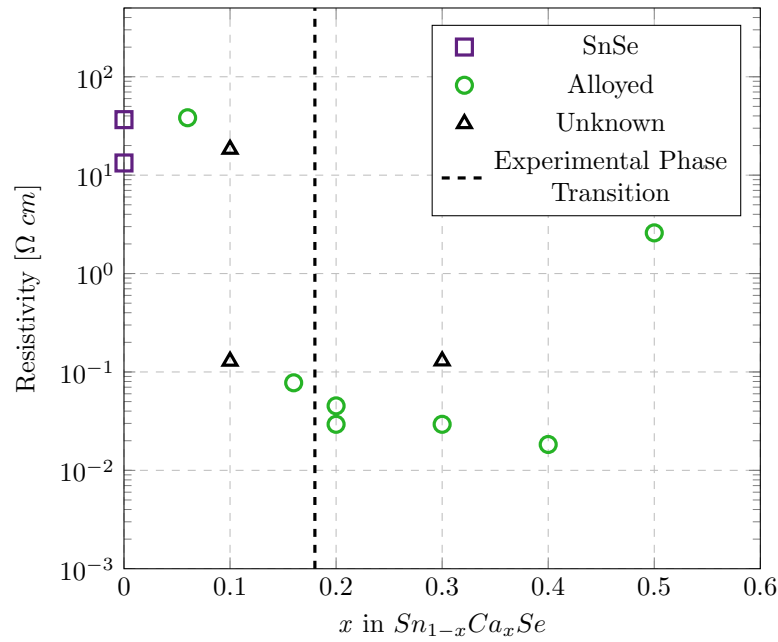


Figure 4.5: Resistivity of the Alloyed Films as a Function of Calcium Doping Concentration

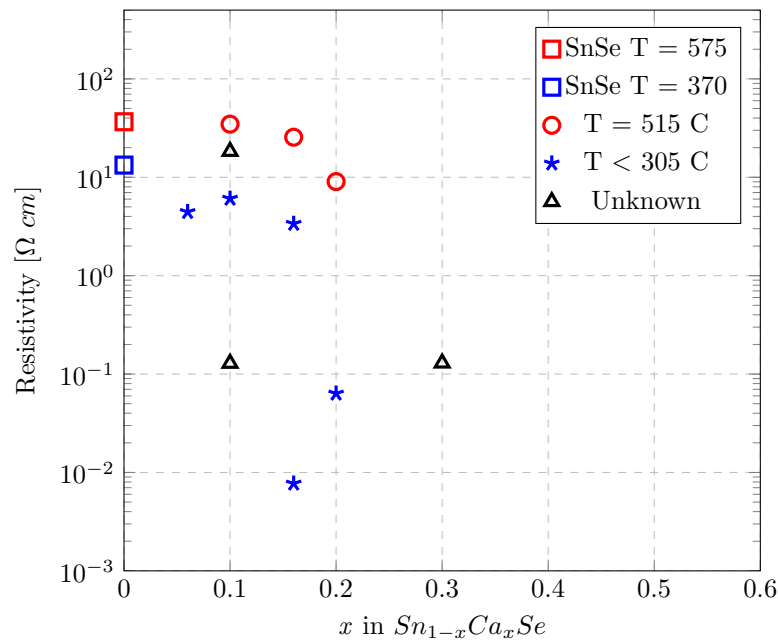


Figure 4.6: Resistivity of the Phase Separated Films as a Function of Calcium Doping Concentration

Figure 4.5 is the resistivity of the alloyed films as a function of calcium concentration x . Pure $SnSe$ has a value in the order of $10 \Omega cm$, and, following the same general trend as the thermoelectric effect, it decreases as you increase the concentration up until the phase transition line. After the phase transition it continues to decrease, then starts to increase again.

Figure 4.6 is the resistivity of the phase separated films as a function of the calcium concentration x . Similar to the carrier density, the high temperature films have values near that of the pure SnSe , while the low temperature films have smaller resistivity values.

4.4 Power Factor

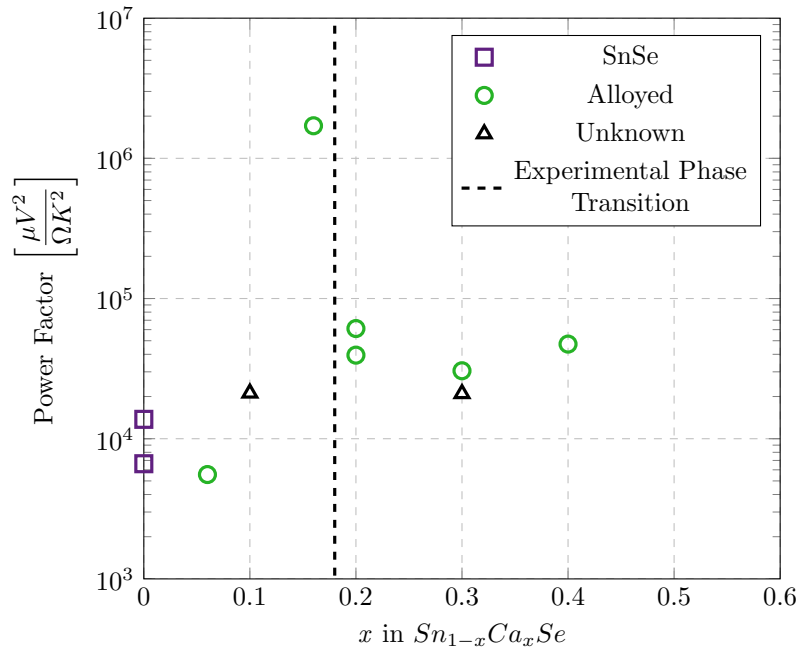


Figure 4.7: Power Factor of the Alloyed Films as a Function of Calcium Doping Concentration

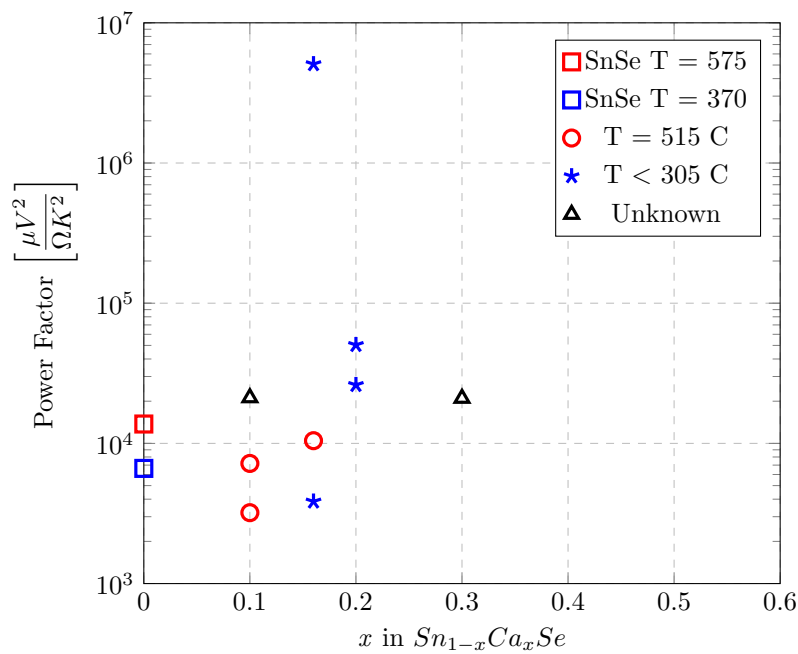


Figure 4.8: Power Factor of the Phase Separated Films as a Function of Calcium Doping Concentration

Figure 4.7 is the power factor of the alloyed films as a function of calcium concentration x . Pure $SnSe$ has a power factor in the order of magnitude $10^4 \mu V^2/\Omega K^2$. The power factor follows a general upward trend with a peak at calcium concentration $x = 0.16$. The trend after the phase transition line is undetermined but is suggestively unchanging.

Figure 4.8 is the power factor for the phase separated films as a function of the calcium concentration x . The high temperature samples are around the same values as pure $SnSe$. The low temperature samples are, on average, larger values than the pure $SnSe$.

4.5 Comparison to Theoretical Band Gap Analysis

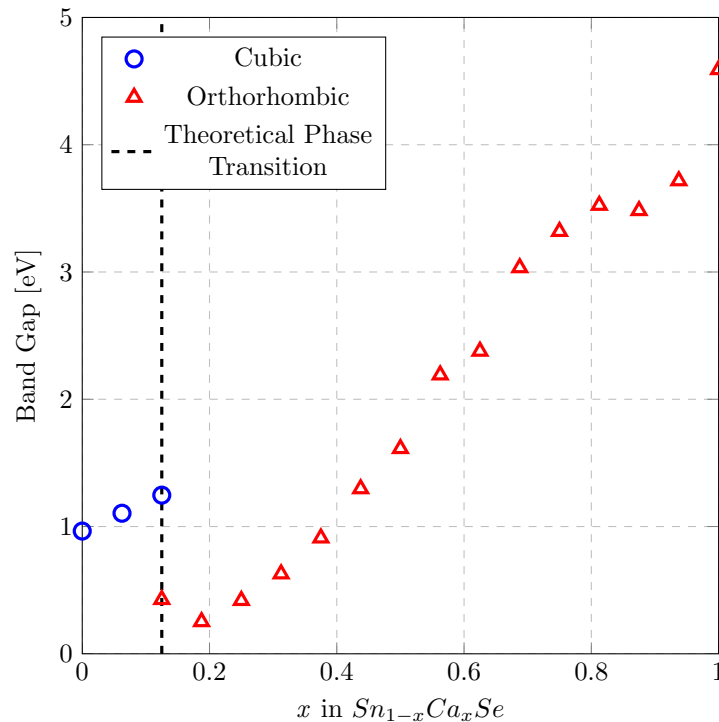


Figure 4.9: Band Gap of the Alloyed Films as a Function of Calcium Doping Concentration [7]

Figure 4.9 shows the theoretical band gap analysis for the alloy $Sn_{1-x}Ca_xSe$. We see a similar trend to the Seebeck coefficient and the resistivity. At the phase transition line, the band gap decreases discontinuously, continues to lower for a small increase in calcium concentration, and increases until it is much larger than the beginning gap. Electrical results are closely tied into the band gap and the structure. The band gap is defined as the amount of energy needed to excite an electron from the valence band to the conduction band. This energy, dependent on the structure and composition of the material, is important in defining the electrical properties.

When we look at the trends in the data, we can see that the Seebeck coefficient and resistivity data closely follow the trend seen in the predicted band gap analysis, while the carrier concentration inversely follows the trend.

4.6 Alloyed Films

There is a large change in electrical properties as the structure changes from orthorhombic to cubic. With every set of data, there is a large discontinuous change, inconsistent with the trends on either side, across

the phase transition line. This is attributed to the change in the structure. When it is energetically favorable to be in the cubic structure instead of the orthorhombic structure, the entire homogeneous structure will have a completely different set of properties.

In isostructural alloying, where the two end members are the same, there is a phenomenon called optical bowing of the band gap. As the doping concentration increases, the band gap changes non-linear. This non-linear change is almost always a small negative deviation from the linear trend. Even with this non-linear change, there is no concentration of the alloy where the band gap is either minimized or maximized [10]. This bowing usually holds true for the electrical properties as well, since band gap and electrical properties are closely related.

The reason heterostructural alloying is such a powerful tool is that the minimum or maximum of the band gap, or electrical properties, does not have to occur at the end members. As we see in all our electrical results, the minimum/maximum does not occur at the pure *SnSe* or *CaSe* compositions, but rather around the phase transition line.

Comparing the Seebeck coefficient and the resistivity, we see that they follow the same trend. In general, metals have extremely low resistivity and a low Seebeck coefficient. So as the resistivity of the sample drops, we expect that the Seebeck coefficient does as well. When we include the carrier density in this comparison, we see that the more carriers we have, the lower the resistivity. Insulators have no free carriers, so they do not, in general, conduct electricity and have no thermoelectric effect, where metals have a very high carrier concentration. For a sample to have a high Seebeck coefficient, it is necessary to have only a small amount of free carriers and limited mobility. The less mobile the carriers, the larger the electric field they will generate when they diffuse and the stronger voltage that electric field will produce.

The power factor is dependent on two different properties, Seebeck coefficient and resistivity. While the Seebeck coefficient and resistivity are related, they have some form of independence. A major goal in semiconductor manufacturing is to maximize the power factor. This is done by maximizing the Seebeck coefficient while simultaneously minimizing the resistivity. Because our Seebeck coefficient and resistivity graphs follow the same trends, we expect there would not be much change in the power factor, and there is not after the phase transition line. Yet, there is still an order of magnitude spike in the value for the power factor around the phase transition line. This is due to a relatively high Seebeck coefficient paired with a relatively low resistivity leading to a large power factor around the phase transition line.

4.7 Phase Separated Films

For the alloyed films, there is no noticeable dependence of the thermoelectric properties on the deposition temperature. For the phase separated films, there is data that suggests the deposition temperature plays a role in the thermoelectric properties at a specific concentration. The two pure *SnSe* films were deposited at 575 C and 370 C. The higher deposition temperature created a more crystalline structure, resulting in a higher quality sample.

When looking at the phase separated alloys, specifically the Seebeck coefficient, we see two distinct trends, one for the high deposition temperature (515 C) and one for the low deposition temperature (between 290 and 320 C). We also see that, for the high temperature samples, the carrier density and resistivity are in the same range as the pure *SnSe* while the low temperature samples are not. Since the sample is phase separated into *SnSe* and *CaSe*, we expect that the properties would not be near that of pure *SnSe* because the sample is contaminated with *CaSe*. Yet, the phase separated films have a low percentage of calcium, so most of the sample is *SnSe*. When the samples are deposited at high temperatures, the phase separated *SnSe* is highly crystalline. This results in overall properties near that of the pure *SnSe* samples. For the lower temperature depositions, the *SnSe* is less crystalline, and therefore the properties are not near that of the pure highly crystalline *SnSe*.

4.8 Raman Spectroscopy

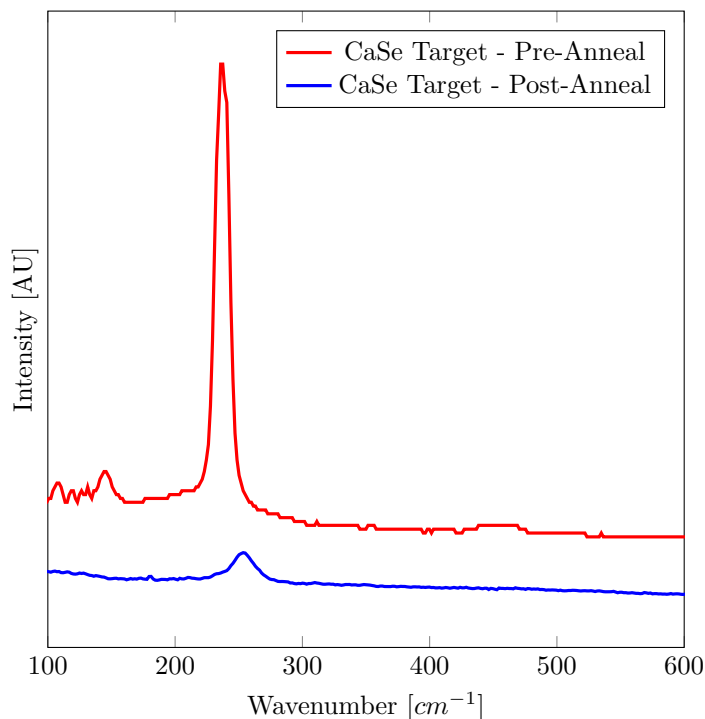


Figure 4.10: Raman Spectra of the CaSnSe Target Pre- and Post-Anneal

Figure 4.10 shows the Raman spectra of the *CaSe* target, used in the PLD process to make the films, before and after an anneal in forming gas to reduce the oxygen present in the sample. Before the anneal, the purity of the sample was questioned because of the large unexpected peak at around 240 cm^{-1} . After the anneal, the peak was much smaller and slightly shifted. While pure *SnSe* has a reference spectrum, the new alloy that was created does not have one, so Raman spectroscopy was not very useful in film characterization. We attempted Raman spectroscopy to see if we could determine if a sample was phase separated or alloyed. Since Raman spectroscopy works on the micron scale, we failed in determining if the whole film was alloyed or phase separated. The one useful piece of information we obtained from the Raman analysis was that our target, used to create the samples, was oxidized. *CaSe* should have no Raman shift due to its cubic nature, and its reference spectrum is a flat line, yet there is a large spike in the data. This corresponds to impurities in the sample that are not pure cubic *CaSe*. The target was annealed to recrystallize it and, when remeasured, the Raman spectrum showed that a large majority of the impurities were removed from the sample. This allowed for creation of higher quality samples.

5 Conclusion

We studied $\text{Sn}_{1-x}\text{Ca}_x\text{Se}$ as a novel homogeneous heterostructural semiconductor alloy. Few studies have focused on what happens to the properties of thin film heterostructural alloys around the phase transition line as they are hard to stabilize into a homogeneous form. We succeeded in creating properly alloyed films at different calcium concentrations and saw that as you cross the phase transition concentration, there is a large discontinuous change in the electrical properties of the semiconductor. Unlike isostructural alloys, the minimum or maximum of the electrical properties does not occur at the pure concentrated ends of the alloy. This leads us to the interesting discovery that alloying heterostructures increased the desired thermoelectric properties, and can potentially be applied to other materials for industrial purposes.

References

- [1] Thermoelectrics. *Department of Physics - University of Oslo*, Nov 2012.
- [2] Blair Bonnent. *Wikipedia Commons - Public Domain*, February 2015.
- [3] Blair Bonnent. *Wikipedia Commons - Public Domain*, June 2006.
- [4] Holly J Butler, Lorna Ashton, Benjamin Bird, Gianfelice Cinque, Kelly Curtis, Jennifer Dorney, Karen Esmonde-White, Nigel J Fullwood, Benjamin Gardner, Pierre L Martin-Hirsch, et al. Using raman spectroscopy to characterize biological materials. *Nature protocols*, 11(4):664–687, 2016.
- [5] Murat Emre Demir and Ibrahim Dincer. Development of an integrated hybrid solar thermal power system with thermoelectric generator for desalination and power production. *Desalination*, 404:59–71, February 2017.
- [6] Joseph P. Heremans. Thermoelectricity: The ugly duckling. *Nature*, 508(7496):327–328, apr 2014.
- [7] Stephen Lany and Aaron Holder Private Communication.
- [8] Cathy Murphy. The Atomic Difference Between Diamonds and Graphite, February 2014.
- [9] Li-Dong Zhao, Shih-Han Lo, Yongsheng Zhang, Hui Sun, Gangjian Tan, Ctirad Uher, C. Wolverton, Vinayak P. Dravid, and Mercouri G. Kanatzidis. Ultralow thermal conductivity and high thermoelectric figure of merit in SnSe crystals. *Nature*, 508(7496):373–377, April 2014.
- [10] Alex Zunger and J. E. Jaffe. Structural Origin of Optical Bowing in Semiconductor Alloys. *Physical Review Letters*, 51(8):662–665, aug 1983.